Research Article

Xinran Ma*

Beyond conventional therapy: Synthesis of multifunctional nanoparticles for rheumatoid arthritis therapy

https://doi.org/10.1515/ntrev-2024-0096
received May 30, 2024; accepted August 7, 2024

Abstract: Rheumatoid arthritis (RA) is a persistent inflammatory illness that causes joint destruction and dysfunction due to the activation of macrophages and the generation of reactive oxygen species. Current therapy choices frequently limit the effectiveness of targeting the inflammatory areas. To reduce inflammation and oxidative stress in RA, this research will create and assess multifunctional nanoparticles that selectively target inflammatory cells and deliver therapeutic medicines. Tannic acid, ferric chloride hexahydrate, methotrexate (MTX), and bovine serum albumin were conjugated using sonication and centrifugation to create the nanoparticles. Folic acid was added to improve the ability to target. Transmission electron microscopy, dynamic light scattering (DLS), UV-vis spectroscopy, and *in vitro* release experiments were used to characterize the nanoparticles. RAW 264.7 macrophage cells were used to test the cellular uptake of the nanoparticles using confocal microscopy and fluorescence-activated cell sorting (FACS). TFMBP-FA achieved 65.56%, and TFMBP reached 68.96%, indicating a high drug delivery rate for the synthesized nanoparticles. Confocal microscopy showed that the TFMBP-FA group had a greater density of fluorescent markers, indicating that the cells effectively targeted and absorbed the inflammatory environment. These results imply that the created nanoparticles may improve how medications are delivered during RA therapy.

Keywords: rheumatoid arthritis, tannic acid-iron based nanoparticle, active targeted therapy, inflammation, ROS scavenging

Abbreviations and expansions

RA	Rheumatoid arthritis
MTX	Methotrexate
DLS	dynamic light scattering
TEM	transmission electron microscopy
FACS	fluorescence-activated cell sorting
RAW	RAW 264.7 – A macrophage cell line used in the experiment
TFMBP-FA	TA-Fe^{3+}-MTX@BSA-PEG-FA – Tannic Acid-Ferric Chloride-Methotrexate@Bovine Serum Albumin-Polyethylene Glycol-Folic Acid
DMARD	disease-modifying antirheumatic drugs
NSAID	non-steroidal anti-inflammatory drugs
GC	glucocorticoids
RONS	reactive nitrogen and oxygen species
ELVIS	extravasation through leaky vasculature and subsequent inflammatory cell-mediated sequestration
FA	folic acid
TA	tannin acid
MOF	meta-organic framework
BSA	bovine serum albumin
ROS	reactive oxygen species
EDC	ethylcarbodiimide hydrochloride
DMEM	Dulbecco's modified eagle medium
PBS	phosphate-buffered saline
NHS	*N*-Hydroxysuccinimide
$NaHCO_3$	sodium bicarbonate
CCK-8	cell counting kit-8
HUVEC	human umbilical vein endothelial cells
FBS	fetal bovine serum
mPEG	methoxy polyethylene glycol
PDI	polydispersity index
FT-IR	Fourier transform infrared
UV-Vis	Ultraviolet-Visible spectroscopy
IVRT	*in vitro* release test
VICTOR TM X4	a multilabel plate reader purchased from Perkin Elmer Inc
LPS	lipopolysaccharides

*** Corresponding author: Xinran Ma,** The Spence School, New York, NY, 10128, United States, e-mail: xinranma354@gmail.com, cma26@spenceschool.org, xinram_ma23@outlook.com

DCFH-DA	dichlorofluorescein diacetate – a fluorescent probe used for detecting reactive oxygen species
ELISA	enzyme-linked immunosorbent assay
FACS	fluorescence-activated cell sorting
qPCR	quantitative PCR
SD	standard deviation

1 Introduction

Rheumatoid arthritis (RA) is an autoimmune disease that can lead to dysfunction and deformity in a patient's joints. RA spreads worldwide, affecting approximately 0.5–1% of people in the United States and Europe [1]. RA is a long-term autoimmune condition that destroys, swells, and inflames joints. Immune cells and pro-inflammatory cytokines are essential players in the inflammatory response directed toward the synovium. Therapeutic approaches to address chronic inflammation and joint deformities include immune cell modification, cytokine suppression, and antioxidants. DMARDs, including biologics, corticosteroids, and NSAIDs, are the current therapy for RA. Although DMARDs delay the course of the disease but can have serious adverse effects, NSAIDs relieve symptoms. Biologic DMARDs are costly and need parenteral administration, which limits accessibility and adherence. However, they target specific immunological pathways. Around 1.3 million adults in the United States suffer from RA, and it has become one of the most common diseases that cause disability. RA is more prevalent in females, and the majority of patients diagnosed with RA are between the ages of 30 and 50 [2]. Its pathological features include synovial hyperplasia, angiogenesis, and bone and cartilage destruction, and it often occurs with symptoms including fever, fatigue, stiffness, deformation, and pain in one or more joints. RA is an incurable disease, and in later stages, patients experience constant pain and face heavy economic burdens. Patients' living conditions are greatly affected by the disease. Therefore, finding a treatment that can restrict the progression of RA in its early stages is essential to its treatment [3,4]. With their effective and targeted delivery mechanism, the suggested nanoparticles seek to enhance the available RA therapies. Encapsulating DMARDs such as methotrexate can be released selectively at inflamed joints while preventing degradation.

Nowadays, the treatment of RA mainly focuses on medicines, physical therapies, and surgeries, which can only relieve the pain temporarily. Medicines like nonsteroidal antiinflammatory drugs (NSAIDs) and disease-modifying antirheumatic drugs (DMARDs), glucocorticoids (GCs), and biological agents are widely used [5]. Because they block COX enzymes, NSAIDs can treat pain and inflammation in RA patients. However, prolonged use of NSAIDs can lead to kidney damage, gastrointestinal ulcers, and cardiovascular problems. The medicine Disease modifying anti-rheumatic drugs (DMARDs), such as methotrexate, target specific immunological pathways; nonetheless, they might have adverse consequences, such as organ damage and immunosuppression, which call for ongoing monitoring. Even though the medicines do have effects on RA, they cannot eliminate inflammation and often come with side effects. Some side effects include diseases affecting the lungs, heart, digestive system, liver, pancreas, and nerve system, which can be potentially fatal [6]. Indirect delivery to the inflamed joints triggers severe side effects, and the tissues get injured when the medicine is delivered to noninflammatory organs.

The past research shows that inflammation plays a vital role in the initiation of RA, and immune cells, inflammatory factors, and reactive nitrogen and oxygen species (RONS) are strongly related to each other in the development of RA [7]. Immune cells detect the healthy tissues as a negative stimulation and start inflammation. Immune cells like macrophages change to M1 polarized phenotype due to the acidic environment in the inflamed joint. M1-type macrophages release abundant inflammatory factors (TNF-α and IL-1β), which are small proteins that can activate the signaling pathway of RONS [8]. Excess RONS increases the immune cells, further enhancing the vicious cycle of RA. RONS can also deteriorate the symptoms. It can stimulate osteoclasts, synovial fibroblasts, and epithelial cells, which are the cells that cause bone erosions, synovitis, and angiogenesis [9]. Therefore, RONS and inflammatory factors are essential targets in the treatment, and conversion of M1-type macrophage is also a strategy in the therapy.

Nanotechnology has been widely used in every aspect of life, and nanoparticles have also been proven to treat various diseases effectively. Due to their small size and specific properties, nanoparticles have been considered a promising strategy for RA therapy. An autoimmune reaction that results in persistent inflammation and joint damage is called RA. By delivering anti-inflammatory medications to inflammatory joints, blocking immune cell activation, and altering the cytokine milieu, nanoparticles can target these pathways and lessen inflammation and joint degradation. For RA therapies, multifunctional nanoparticles provide targeted distribution, regulated release, multifunctionality, and fewer dosing cycles. They can be designed to improve patient compliance, keep therapeutic doses at optimal levels, and incorporate imaging agents for effectiveness monitoring. Nanoparticles can be either passively or positively

accumulated in the inflamed joint. Extravasation through leaky vasculature and subsequent inflammatory cell-mediated sequestration (ELVIS) affects the accumulation of small-size nanoparticles in the joint. Also, M1-type macrophages have overexpressed receptors on the cell membrane. For example, the folate receptor in the membrane is overexpressed, so the nanoparticles decorated with folic acid (FA) would actively accumulate in a place with many M1 macrophages. Active and passive targeting help nanoparticles directly deliver to the inflamed joint, leading to a high therapeutic effect and a low risk of getting side effects. Integrating medicinal, diagnostic, and targeted functions into a single nanoscale entity is known as multifunctional nanoparticles, an emerging area of nanotechnology. They reduce adverse effects, increase specificity, and improve therapy effectiveness. The synthesis process includes conjugation or encapsulation of the medicinal substance, surface changes, and core components.

Tannin acid (TA) is a type of polyphenol and is an FDA-approved medicine today. Tannin acid has an abundant trihydroxybenzene group, which enables TA to develop versatile functions [10–12]. TA can attenuate oxidative stress and eliminate RONS due to its effect on antioxidative activity. Metal-organic frameworks (MOFs) consist of metal clusters and organic ligands to form one-, two-, or three-dimensional structures [13]. TA and iron(III) chloride MOFs can build the structure of the experimental nanoparticle from the bottom up. Bovine serum albumin (BSA) is the globulin from bovine serum coated around the nanoparticles, and it can increase the solubility and stability of nanoparticles [14,15]. Inside the tannin nanoparticles, a type of DMARDS medicine, methotrexate (MTX), will be loaded.

MTX would be released after the nanoparticles are either passive or actively accumulated in the inflamed joint. Direct delivery of MTX can reduce inflammation by getting rid of reactive oxygen species (ROS) and RNS and can reduce the risk of side effects [16]. The nanoparticles can reduce the RONS and inflammatory factors in the joint, decreasing the amount of M1-type macrophage and relieving inflammation [17–19]. Therefore, the nanoparticles demonstrate an effective treatment for RA therapy. RA is exacerbated by reactive oxygen and nitrogen species (RONS), which lead to tissue damage, persistent inflammation, and inflammation. Antioxidants, anti-inflammatory medications, and nanoparticles are therapeutic approaches that lower inflammation and oxidative stress. Effective treatment plans for RA have been made possible by our growing understanding of the disease's pathophysiology; nonetheless, issues with systemic toxicity, bioavailability, and insufficient response still exist. Nanomedicines have been created to overcome these drawbacks with their controlled characteristics, customized drug release patterns, and active targeting. Recent developments in antigen-specific tolerance, pro-resolving therapy, and immunometabolism modulation in nanomedicines for RA treatment are covered in this review [20]. Two chronic inflammatory joint illnesses are osteoarthritis and RA. Pain relief and cartilage repair are achieved using conventional medications.

However, conventional medications have drawbacks, including the cartilage barrier and quick drug elimination. Controlled drug release, extended retention times, and improved penetration into joint tissue are some ways that nanoparticles might increase the effectiveness of intra-articular injections. With an emphasis on tissue/cell targeting and controlled drug release, this review examines nanoparticle-based therapeutics for managing OA and RA [21]. This study investigates the viability of predicting cardiovascular risk in people with RA using long-term blood samples. Assessing biomarker stability and lipid profiles integrates conventional risk factors with markers unique to RA. Disease activity indexes and cardiovascular outcomes are studied using longitudinal data analysis. By filling scientific gaps and emphasizing clinical translation, the project seeks to enhance patient outcomes, boost cardiovascular risk prediction, and enable customized medicines [22].

2 Materials and methods

2.1 Materials and cells

2.1.1 Materials

Tannin acid (TA) was obtained from Shanghai Titan Scientific Co., Ltd. (CAS: 1401-55-4), and iron(III) chloride hexahydrate ($FeCl_3{\cdot}6H_2O$) was from Sigma-Aldrich Co., Ltd. (CAS: 10025-77-1). BSA was purchased from Merck Science and Technology Co., Ltd. (CAS: 9048-46-8), and methotrexate (MTX) was purchased from Adamas Pharmaceutical Co., Ltd. (CAS: 59-05-2). 1-(3-Dimethylaminopropyl)-3-ethylcarbodiimide hydrochloride (EDC) and *N*-hydroxysuccinimide (NHS) were gained from Tokyo Chemical Industry Co., Ltd. with (CAS: 25952-53-8) and (CAS: 6066-82-6). FA-PEG2000-NH_2 and mPEG2000-NH_2 were purchased from Ponsure Biological Co., Ltd. Dulbecco's modified eagle medium (DMEM) and phosphate-buffered saline (PBS) were obtained from Thermo Fisher Scientific Inc. Reagents employed in the manufacture of nanoparticles are NHS and EDC. ToEDC activates carboxyl groups with amines to couple them and produce amide bonds. NHS produces a stable intermediate, which improves this coupling efficiency. The creation of nanoparticles requires both reagents. Sodium bicarbonate ($NaHCO_3$) and *N*-hydroxysuccinimide (NHS) esters were purchased from Shanghai Saint-Bio Co., Ltd. TMB ELISA substrate

solution was from Beyotime Co., Ltd. CCK-8 cell proliferation and cytotoxicity detection kit was purchased from Dalian Bergolin Co., Ltd. The CCK-8 cell proliferation and cytotoxicity detection kit from Dalian Bergolin Co., Ltd. assesses the safety and biocompatibility for possible therapeutic applications and evaluates the viability and cytotoxicity of cells exposed to nanoparticles. This allows comparison across experimental conditions and the determination of cytotoxic effects.

2.1.2 Cells

The macrophage cell line (RAW 264.7) and human umbilical vein endothelial cells (HUVEC) used in the experiment were from the Shanghai Cell Centre of the Chinese Academy of Sciences. RAW 264.7 and HUVEC were cultured in DMEM medium composed of 10% fetal bovine serum (FBS) and 1% streptomycin and penicillin. The cells were stored in a CO_2 incubator purchased from Thermo Fisher Scientific Inc.

2.2 Synthesis of TA-Fe^{3+}-MTX@BSA

Using an electronic balance, 102.5 mg of 95% tannic acid (TA), 100.6 mg of 98% ferric chloride hexahydrate ($FeCl_3{\cdot}6H_2O$), 40.6 mg of 98% BSA, and 5.1 mg MTX were weighed. TA and $FeCl_3{\cdot}6H_2O$ were dissolved in 10 mL of deionized water and BSA was dissolved in 5 mL. MTX was added into a 10 mg/mL ferric chloride solution and reacted for 10 min using an ultrasonic reactor. To treat RA, methotrexate (MTX) and ferric chloride are mixed to form a stable, targeted nanoparticle delivery system. This combination guarantees that MTX is selectively administered to inflamed joints, improving its stability and solubility, which increases efficacy and decreases adverse effects. After the reaction, 10 mg/mL of TA solution was added, stirred, and reacted for 10 min using an ultrasonic reactor. After that, 8 mg/mL of BSA solution was added and reacted for 10 min. The overnight reaction was carried out under ice bath conditions for 24 h. With minimum equipment needed, overnight ice bath reactions provide temperature control, stability, yield, purity, practicality, safety, and enhancement of selectivity and stability while minimizing the danger of overheating and avoiding decomposition. Samples were collected by centrifugation at 14,000 rpm for 15 min and then cleaned with deionized water three times. A drying machine dried the samples, and the nanoparticle TA-Fe^{3+}-MTX@BSA was obtained (Figure 1). To preserve the uniformity, stability, biocompatibility, and purity of the nanoparticles, avoid aggregation, and improve performance, the sample must be cleaned three times with deionized water following centrifugation.

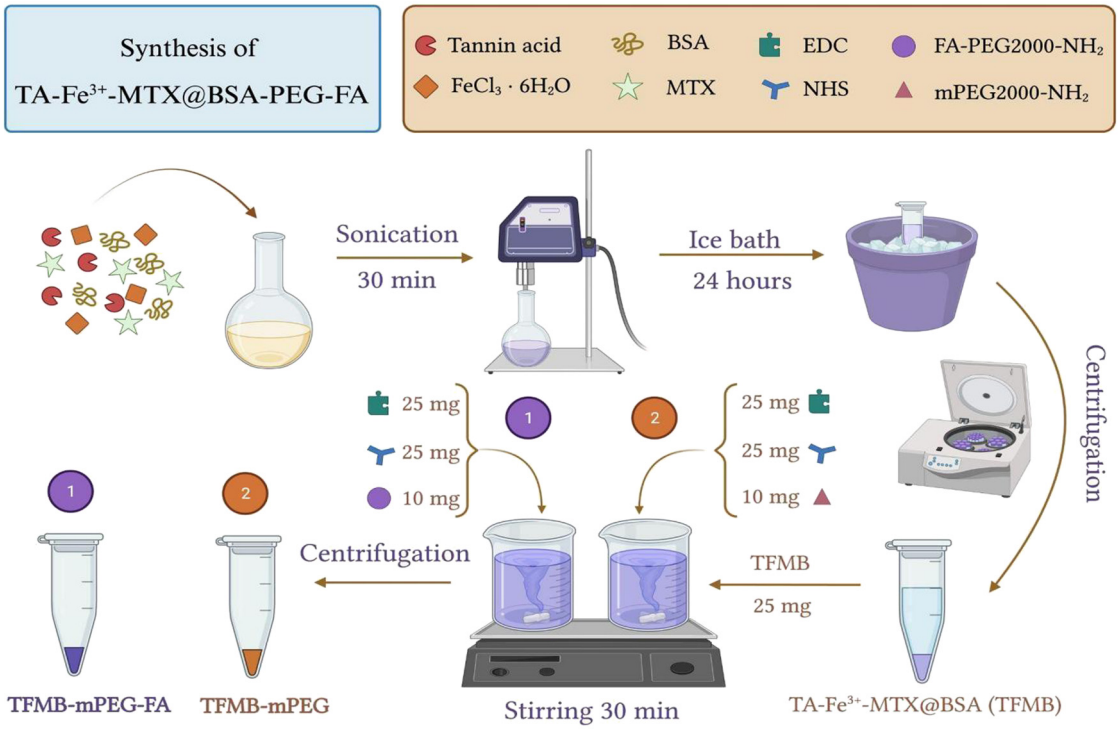

Figure 1: Synthesis of TA-Fe^{3+}-MTX@BSA-PEG-FA and TA-Fe^{3+}-MTX@BSA-mPEG.

2.3 Synthesis of TA-Fe^{3+}-MTX@BSA-mPEG/TA-Fe^{3+}-MTX@BSA-PEG-FA

Two nanoparticles with and without folic acid would be synthesized separately. A magnetic stirrer works well for nanoparticle mixes because of its practical efficiency, repeatability, uniform mixing, and temperature control. Even component distribution is guaranteed, reagent interaction is maximized, temperature is maintained consistently, stirring speeds may be adjusted, and contamination hazards are reduced. The capacity to prevent aggregation, stabilize surface chemistry, employ moderate functionalization techniques, and inherent stability all contribute to the shape maintenance of nanoparticles. Surface treatments that provide a hydration layer, stop aggregation, and improve stability include BSA and PEG. Two portions of TA-Fe^{3+}-MTX@BSA weighed about the same mass (25.6 and 25.0 mg), and the nanoparticles were put into two separate bottles. Two portions of EDC (25.1 and 25.3 mg) and two portions of NHS (25.3 and 25.8 mg) were added to the bottle. A magnetic stirrer was used to stir the two bottles of mixture for 30 min. A total of 10.3 mg of FA-PEG2000-NH_2 and 10.2 mg of mPEG2000-NH_2 were weighed and dissolved with deionized water in separate centrifuge tubes. To synthesize TFMBP-FA and TFMBP, FA-PEG2000-NH_2 solution and mPEG2000-NH_2 solution were mixed with TFMBP in separate bottles. After 3 h of reaction, the samples were collected thrice by centrifugation at 14,000 rpm for 15 min. Finally, the nanoparticles were dried and collected with 10.1 mg TFMBP and 11.8 mg TFMBP-FA. The yield rate for TFMBP was 40.4%, and that for TFMBP-FA was 47.2%.

2.4 Preparation and characterizations of TA-Fe^{3+}-MTX@BSA-PEG-FA

The nanoparticles TFMBP-FA and TFMBP were synthesized using the aforementioned procedures. After TFMB was synthesized by conjugating tannin acid, $FeCl_3{\cdot}6H_2O$, BSA, and MTX, two nanoparticles were created separately by adding FA-PEG2000-NH_2 and mPEG2000-NH_2. FA-PEG2000-NH2 and mPEG2000-NH2 are nanoparticles that target cells that express the folate receptor, thereby improving medication delivery. Active targeting, improved drug specificity, stability, solubility, and dual functionalization are among the benefits they provide, giving designers more freedom to create nanoparticles with various therapeutic effects and processes. The successful conjugation of the nanoparticles was confirmed by transmission electron microscopy (TEM), DLS, UV-vis, FT-IR characterization, and *in vitro* release test. Numerous tests, including TEM, DLS, UV-vis, FT-IR, and *in vitro* release experiments, visually assess the size, shape, morphology, aggregation, optical characteristics, and molecular structure to confirm the production of nanoparticles. Their effectiveness as drug delivery devices is ensured by the fact that these tests also yield data on hydrodynamic diameter and surface charge for stability evaluation.

TEM examined the feature and surface morphology. The size of the particles, zeta potential, and polydispersity index (PDI) were measured using dynamic light scattering (DLS). One method for determining a nanoparticle's size and zeta potential is DLS. A detector is used to analyze the light scattered off the nanoparticles by a laser beam. The hydrodynamic diameter may be computed using the zeta potential and diffusion coefficient. DLS analyzes hydrodynamic diameter and particle size distribution, utilizing scattered light intensity variations. This technique is vital for formulation development, stability studies, and quality control in nanoparticle characterization. The method applies the Stokes–Einstein equation and the polydispersity index to analyze particle size distribution. The UV-vis and infrared absorbance spectra were determined by UV-Vis spectroscopy and infrared FT-IR spectroscopy. FT-IR spectroscopy and UV-Vis spectroscopy are two methods that provide complimentary data in various scientific domains. FT-IR concentrates on vibrational transitions in the infrared spectrum, whereas UV-Vis concentrates on electronic transitions in the ultraviolet and visible areas. Also, the drug delivery system's safety, efficacy, and quality were assessed by an *in vitro* release test (IVRT).

2.5 *In vitro* cytotoxicity study

RAW 264.7 and HUVEC cells were seeded in a 96-well plate at 5,000 cells/healthy density and cultured in a humidified incubator at 37°C with 5% CO_2 for 24 h (the cell density reached approximately 70%). Nanoparticles are trained by incubating them at certain temperatures and times to enable effective drug encapsulation and functionalization while regulating their physicochemical characteristics. This optimizes the stability, size, and drug-loading efficiency of the nanoparticles. The cell density is measured using a cell counting board. Meanwhile, the medium with cell solutions is prepared and diluted to different concentrations (0, 50, 100, 150, 200, 250, and 300 μg/mL). Then, the old cell culture medium is discarded in the healthy plate, 100 μL of the culture is added to the aforementioned medium containing synthesized nanoparticle materials at different concentrations, culture medium with nontargeting nanomaterials is

added to the control group, and neither cells nor materials are added to the blank group. After the cells have grown in the incubator for 24 h, the old medium is discarded and it is replaced with a fresh medium containing 10% CCK-8 reagent. A total of 10 μL is added to each well, and the plates are incubated for 1 h in the incubator. A microplate reader is used to measure the absorbance of the culture medium in each well at a wavelength of 450 nm. The method of measuring absorbance at 450 nm is a sensitive, specific, and standardized approach to measuring cell viability. It is also connected with forming formazan dye and yields quantitative data that are easy to interpret, repeatable, and compatible with various tests. Four wells were set up as parallel samples for each concentration of the experimental, control, and blank groups. The VICTOR TM X4 multilabel plate reader was purchased from Perkin Elmer Inc.

2.6 Cellular uptake study

Raw 264.7 cells were seeded in a 96-well plate and cultured in a 5% CO_2 incubator. A total of 10 μL of fluorescent conjugation (NHS-ester) and 50 μL of 1 M $NaHCO_3$ were added to the nanoparticles separately. The mixtures were stirred in an essential condition for 2 h and then centrifuged for 15 min at 14,000 rpm. A total of 100 μL RAW 264.7, 3,900 μL DMEM, 1 μL LPS, and 0.1 μL of the nanoparticles were added to each well in the plate. 500 μL PBS was added to the solution, and the solution in each well was removed and placed into a 1.5 mL microcentrifuge tube, followed by centrifugation for 3 min at 1,200 rpm. Finally, 1 mL of PBS was added to each centrifuge tube, and each tube was analyzed with flow cytometry. The confocal microscopy images were taken with Alexa Fluorescence 488.

2.7 RONS scavenging activity assay

The RONS scavenging activity assay improves sensitivity and accuracy by eliminating excess DCFH-DA from cells. To achieve consistency and trustworthy data for assessing RONS scavenging activity, this minimizes interference, removes nonspecific binding, decreases background noise, and guarantees that the fluorescence is from intracellular RONS. RAW 264.7 cells were collected and re-suspended, adjusted to a density of 10^6 cells/mL, and seeded into 3.5 cm cell culture dishes according to the tested group (LPS+, TFMBP, LPS+TFMBP, TFMBP-FA, LPS+TFMBP-FA). A total of 10 μL of LPS and 2 μL of the nanoparticles were added into the dishes and placed in the 5% CO_2 37°C incubator for 24 h. Each cell culture dish was stained with 5 μM of ROS probe DCFH-DA and cultured in an incubator under the same conditions for 20 min. Then, the cell culture dishes were washed three times with PBS to remove excess DCFH-DA outside the cells. Finally, a scanning laser confocal microscope was applied to observe and record the samples. High-resolution imaging is possible using scanning laser confocal microscopes, capturing minute details for analysis and depth perception. They employ fluorescent labeling, high-contrast pictures, and quantitative analysis to evaluate the quantity and distribution of nanoparticles. They record time-lapse videos for live cell imaging and temporal dynamics.

2.8 Inflammatory factors scavenging study

All reagents and samples returned to room temperature (18–25°C) before use. RAW 264.7 was seeded into 3.5 cm cell culture dishes according to the tested group (LPS+, TFMBP, LPS+TFMBP, TFMBP-FA, LPS+TFMBP-FA). A total of 10 μL of LPS and 2 μL of the nanoparticles were added into the dishes and placed in the 5% CO_2 37°C incubator for 24 h. In a 96-well plate, two precoated plates were prepared, and 100 μL of cell solution was added to each well. The plate was wrapped with tape and placed in the fridge overnight. The solution in the well was discarded and washed four times with ELISA wash buffer. Each well was washed with a wash buffer (300 μL) using a multichannel pipette. After the last wash, the residual wash buffer was removed by pipetting or pouring. The plate was turned upside down, and it was blot dried with a clean paper towel. 100 μL of the prepared TNF-α and IL-1β detection antibody was added to each well. The wells were covered and incubated for 30 min at room temperature. 100 μL of TMB one-step substrate reagent was added to each well. The wells were covered and incubated in the dark at room temperature for 10 min with gentle shaking. The solution on the plate turned blue. 100 μL of stop solution (H_2SO_4) was added to each well, and the solution turned yellow. A microplate reader at 450 absorbance was used to examine the plate.

3 Results and discussions

3.1 Synthesis of TA-Fe^{3+}-MTX@BSA-PEG-FA

Nontargeting material TA-Fe^{3+}-MTX@BSA (TFMB) was synthesized by conjugating tannin acid, ferric chloride hexahydrate,

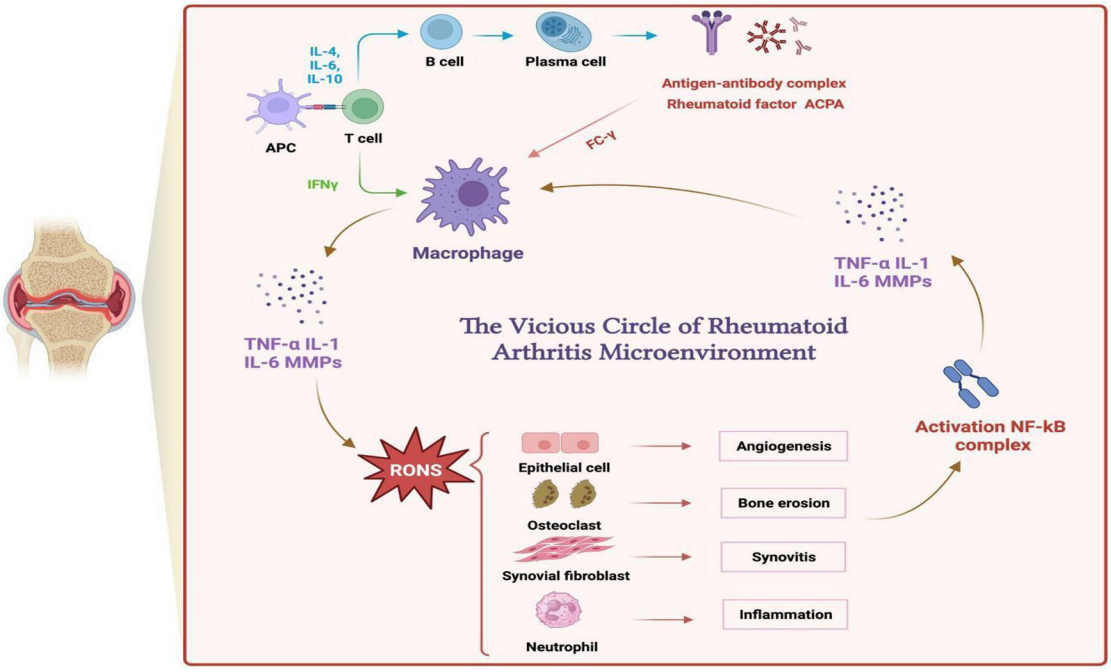

Figure 2: Effect of RONS in inflamed joints and the vicious circle of RA.

MTX, and BSA through sonication and centrifugation. The nanoparticle TA-Fe^{3+}-MTX@BSA-PEG-FA (TFMBP-FA) was synthesized by combining folic acid with TFMB, and NHS and EDC were used to help conjugation. Two different kinds of nanoparticles were created: TA-Fe^{3+}-MTX@BSA-PEG-FA and TA-Fe^{3+}-MTX@BSA-mPEG. The folic acid-containing nanoparticles were designed to improve macrophage targeting in inflammatory joints by binding to overexpressed folate receptors. The successful synthesis of the nanoparticle was qualified by TEM. From TEM graphs, the polydisperse nanoparticles formed various distributions through overlapping due to their small size and formed a web structure (Figure 3a and b). mPEG2000-NH_2 was attached to the surface of the nanoparticles and formed TA-Fe^{3+}-MTX@BSA-PEG (TFMBP). By adding folic acid, the polydisperse arrangement of TFMBP-FA is retained in a web structure (Figure 3c and d). With or without folic acid, the nanoparticles maintained the same shapes, affirming the basic structure of the nanoparticle. Compared to nontargeted nanoparticles and conventional treatments, the study demonstrates that multifunctional nanoparticles can enhance methotrexate delivery and efficacy in RA therapy. Targeted folic acid nanoparticles demonstrated superior accumulation in inflamed joints, reduced systemic toxicity, and improved therapeutic outcomes.

3.2 Preparation and characterization of TA-Fe^{3+}-MTX@BSA-PEG-FA

Both TFMBP and TFMBP-FA were measured using dynamic light catering (DLS). DLS measures the size and zeta potential of the nanoparticles, and the zeta potential indicates the stability of the particles [23]. When a zeta potential that is close to 0 (*e.g.* ± 5 mV) would be considered unstable, and as the absolute value increases, the particle becomes more stable. A nanoparticle with zeta potential ± 10 mV is considered charged neutral. A negative zeta potential value indicates that the material would not combine with other proteins and molecules, which helped the active targeting [24]. TFMBP had an average size of 171.7 ± 1.13 nm, and its zeta potential was −5.24 (Figure 4a and c). TFMBP-FA's size average was 286.5 ± 1.89 nm, and its zeta potential was −12.4 (Figure 4b and c). TFMBP-FA had a relatively larger size compared to TFMBP. The conjugation of folic acid on the nanoparticle's surface increased the size. TFMBP-FA's zeta potential was ~10 mV, and TFMBP's zeta potential was ~5 mV (Figure 4c). The change in the zeta potential shows that folic acid lowered the zeta potential, which led to higher stability and better biological application.

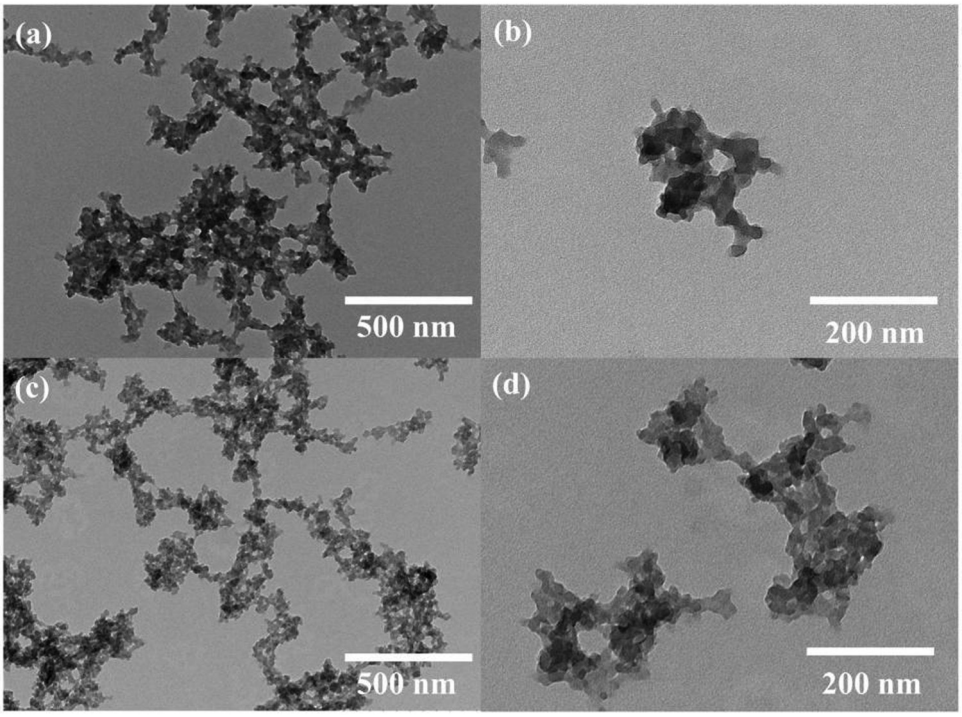

Figure 3: TEM micrographs of (a) TFMBP (scale bar = 500 nm) and (b) TFMBP (scale bar = 200 nm). TEM micrographs of (c) TFMBP-FA (scale bar = 500 nm) and (d) TFMBP-FA (scale bar = 200 nm).

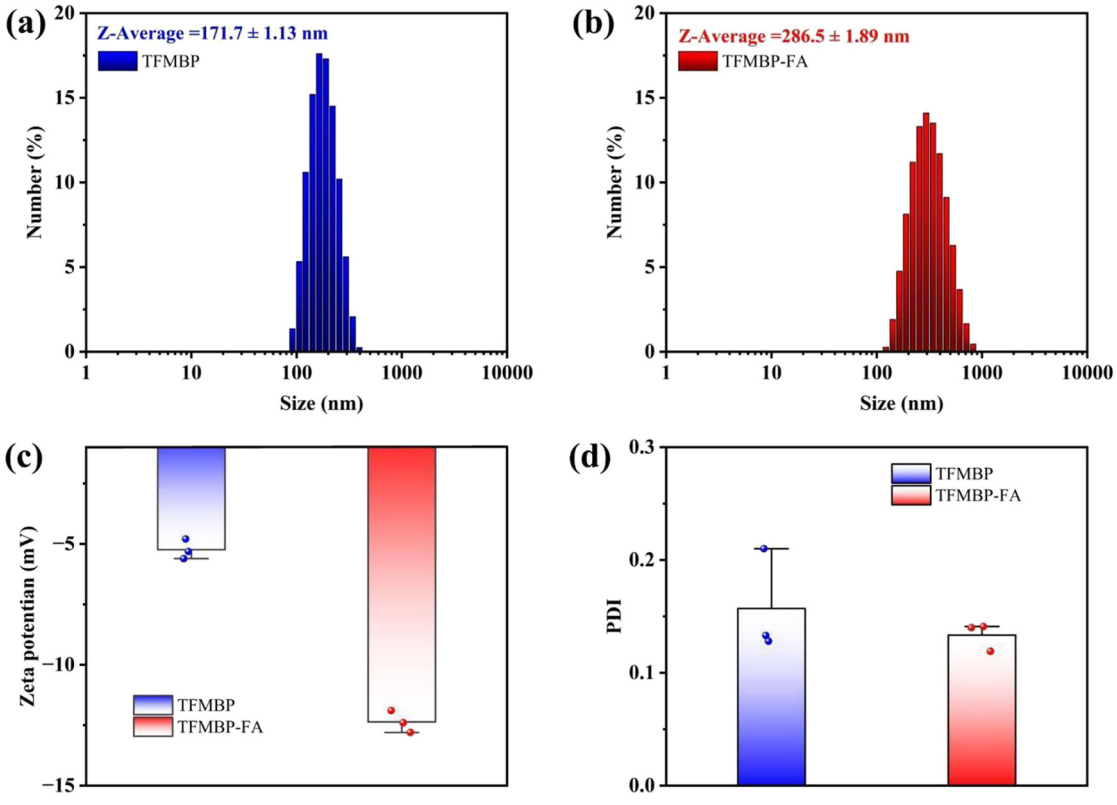

Figure 4: Dynamic light scattering graphs represent (a) TFMBP size and (b) TFMBP-FA size. (c) Zeta potential and (d) the polydispersity index (PDI) of TFMBP and TFMBP-FA.

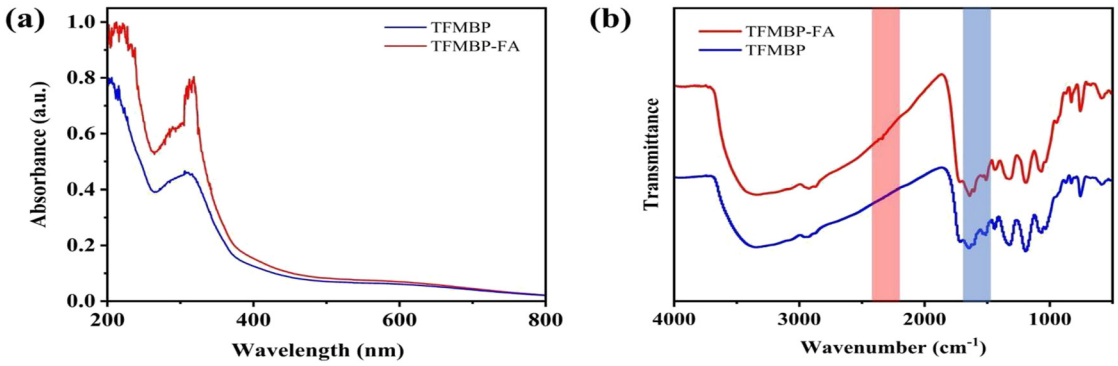

Figure 5: (a) Ultraviolet-visible (UV-vis) spectroscopy analysis of TFMBP and TFMBP-FA. (b) Fourier transform infrared spectroscopic (FTIR) analysis of TFMBP and TFMBP-FA.

The polydispersity index (PDI) displays the heterogeneity of the particles based on their size [25]. When the index is closer to 0.0, the size distribution is more petite and uniform. TFMBP has a PDI of 0.157, and TFMBP-FA has a PDI of 0.133 (Figure 4d). TFMBP-FA has a smaller PDI than TFMBP, which indicates that the size of TFMBP-FA is approximately uniform. By adding the folic acid group, the size of the nanoparticle increased, the PDI decreased, and the stability of the material also increased. Therefore, the nanoparticles were proved to be suitable for biological application.

TFMBP and TFMBP-FA showed a solid absorbance to the ultraviolet light, which has a peak absorbance at ~300 nm wavelength (Figure 5a). The wavelength of UV or visible light absorbed or transmitted through the particle was collected and compared by ultraviolet-visible spectroscopy.

Nanoparticles were characterized by Fourier transform infrared (FTIR) spectroscopy, and their absorbance to infrared radiation by FTIR spectroscopy was tested [26]. FTIR spectroscopy is a method that helps detect chemical bonds and functional groups to characterize nanoparticles. A suspension or pellet must be prepared to measure infrared radiation. The data must then be converted into an infrared spectrum with particular chemical vibration peaks. FTIR spectroscopy is used to determine molecular structures and identify chemical species. It is also used to study nanoparticles' surface effect and identify the functional groups' presence [27]. The characteristic absorbance peaks for TFMBP-FA at 945 cm^{-1} (attributed to the N–H motions in FA), 1,480 cm^{-1} (absorption band of the phenyl ring in FA), and ~1,900 cm^{-1} (amide bond, H–N–C═O bending vibrations from FA) correspondingly appeared in the TFMBP nanoparticle (Figure 5b).

The nanoparticles were characterized by an *in vitro* release test (IVRT), and the examination is to assess the safety, efficacy, and quality of nanoparticle-based drug (MTX) delivery systems [28]. IVRT can reflect the combined effects of several physicochemical characteristics, particle or droplet size, viscosity, microstructure arrangement of the material, and state of aggregation of the dosage form [29]. The standard curves were measured at five different MTX concentrations. The peak absorbance of various MTX concentrations was at 390 nm (Figure 6a). As the MTX concentration increases, the absorbance of UV light also increases (Figure 6b). According to the Beer-Lambert Law, absorbance

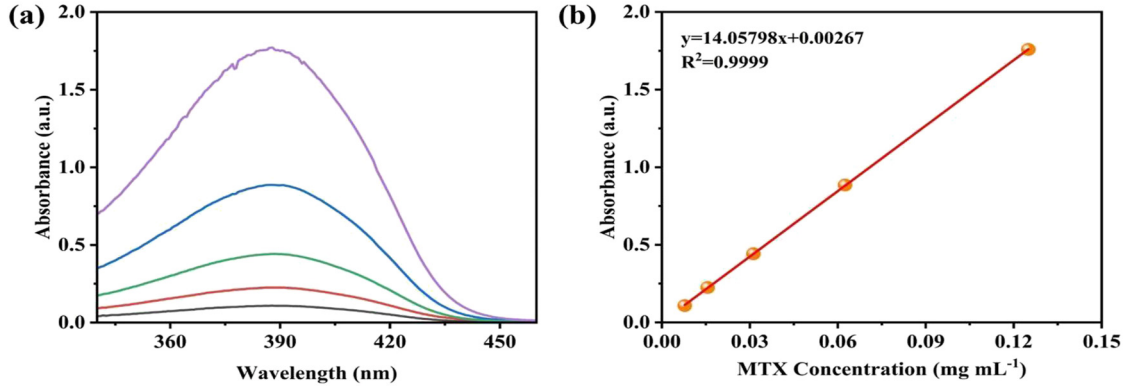

Figure 6: (a) Absorbance vs wavelength graph of five different concentrations of MTX and (b) standard curve of drug release.

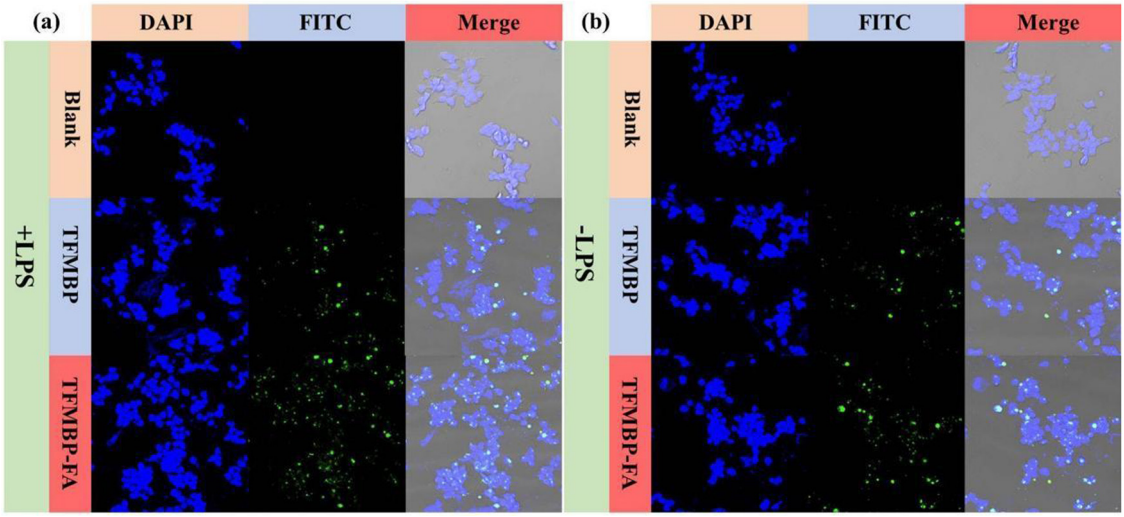

Figure 7: Fluorescent confocal microscopy images of (a) RAW 264.7 cells treated with TFMBP and TFMBP-FA and (b) activated RAW 264.7 cells treated with TFMBP and TFMBP-FA.

and route length are closely correlated with MTX concentration. In the UV spectrum, MTX exhibits distinct absorption peaks at about 300 nm. Higher absorbance results from more molecules absorbing UV light as MTX concentration rises. This connection makes accurate measurement and medication release monitoring possible. The R^2 value is 0.9999, which shows the data and equation fit properly. The R^2 value shows the correlation between the data and the line equation. According to the standard curve equation $y = 14.05798x + 0.00267$, the drug delivery rate for TFMBP-FA is 65.56%, and the drug delivery rate for TFMBP is 68.96%, which indicates that the nanoparticles would be able to be delivered to the inflammation place with enough MTX.

3.3 *In vitro* cellular uptake

The cellular uptake of TFMBP-FA and TFMBP was assessed by using the RAW 264.7 cells. The cells were divided into six different experimental groups: LPS−, LPS+, TFMBP, LPS+TFMBP, TFMBP-FA, and LPS+TFMBP-FA. Lipopolysaccharides (LPS) can transform M0 macrophage to M1 type macrophage, which can mimic the inflammatory environment in the experiment. The cellular uptake of the materials was measured by fluorescence-activated cell sorting (FACS) and confocal microscopy because both techniques used lasers as part of the measurement, and fluorescent conjugation (NHS-ester) was added to the nanoparticles. Among the confocal microscopy images, both TFMBP and TFMBP-FA images show the abundant presentation of the fluorescent markers, indicating that the cells can take the nanoparticles (Figure 7a and b). In the TFMBP-FA images, the fluorescent markers have a higher density, which shows the effectiveness of FA, which functions as an actively targeted material. Increased fluorescence marker density in TFMBP-FA pictures enhances signal strength, sensitivity, and nanoparticle identification, allowing for more precise quantification and lucid visualization. However, it also brings significant difficulties, such as improved photobleaching and background fluorescence, which call for optimization to strike a compromise between signal strength and noise. The blank group did not present any fluorescent markers because they did not add any materials. Assuring fluorescence specificity, removing artifacts, and bolstering the validity of findings by proving rigorous experimental design and effects attributable to experimental variables are just a few reasons the statement highlights the importance of the blank group (Figure 7a and b).

According to the data from FACS, the fluorescence intensity was differentiated due to the materials they added. TFMBP-FA and LPS+TFMBP-FA had a fluorescence intensity of ~10^5; TFMBP and LPS+TFMBP had a fluorescence intensity of ~10^4; and LPS− and LPS+ had a fluorescence intensity of ~10^3 (Figure 8). The nanoparticles with folic acid had the highest value among the groups, whether with LPS+ or LPS−. Nanoparticles with folic acid can be better uptake by the cells, as proved in the data, and the active targeting capability of TFMBP-FA is demonstrated.

3.4 *In vitro* cytotoxicity

The cell counting kit-8 (CCK-8) was used to measure the cell viability and cytotoxicity of the material, which is essential

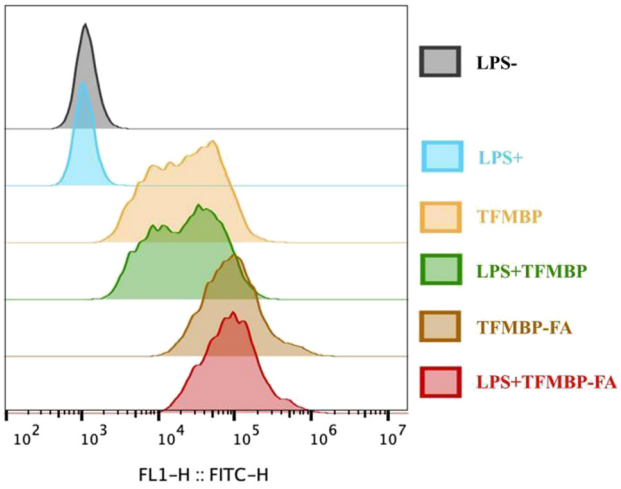

Figure 8: Flow cytometry images of RAW 264.7 cells and activated RAW 264.7 cells treated with TFMBP or TFMBP-FA.

to maintaining cell proliferation and cellular health [30]. CCK-8, under the condition of existing electron carriers, is reduced by the dehydrogenase inside the cell into soluble formazan that dyes the culture solution orange. The quantity of formazan produced is directly proportional to the number of living cells.

The cytotoxicity of the material TFMBP-FA was tested by RAW 264.7 and HUVEC cells. In HUVEC cells and RAW 264.7 with normal and activated macrophages, the cell viability demonstrated a concentration-dependent trend; as the concentration increased, the cell viability decreased. In HUVEC cells, the cell viability is above 100% when both materials are at 50 mM (Figure 9a). The cell viability of TFMBP-FA was significantly higher than TFMBP until 150 mM. In RAW 264.7 cells with normal macrophages, the cell viability of TFMBP-FA at 50, 100, 150, and 200 mM were ~90% (Figure 9b), and the rate of TFMBP decreased gradually. Starting at 100 mM, the cell viability rates of TFMBP-FA were higher than TFMBP. In RAW 264.7 cells with activated macrophages, cell viability was above 50% at 50 mM for both nanoparticles (Figure 9c). Compared to the cell viability in normal and activated macrophages, cells with activated macrophages had a higher viability rate. Because tannin acid and MTX would react with RONS and inflammatory factors, the reaction eliminates the remainder of the nanoparticles (Figure 10). Fewer nanoparticle portions would remain, leading to lower cytotoxicity to the cells. 300 mM had the lowest viability rate, and 50 mM had the highest (~100 mM) in three experiments, which is suitable for biological application based on safety and biosecurity. Therefore, 50 mM was used as the standard concentration in the later experiment.

3.5 ROS scavenging capability

During inflammation, immune cells release inflammatory factors (cytokines) to activate various oxidases that produce a large amount of ROS [31]. The capability of TFMBP-FA to

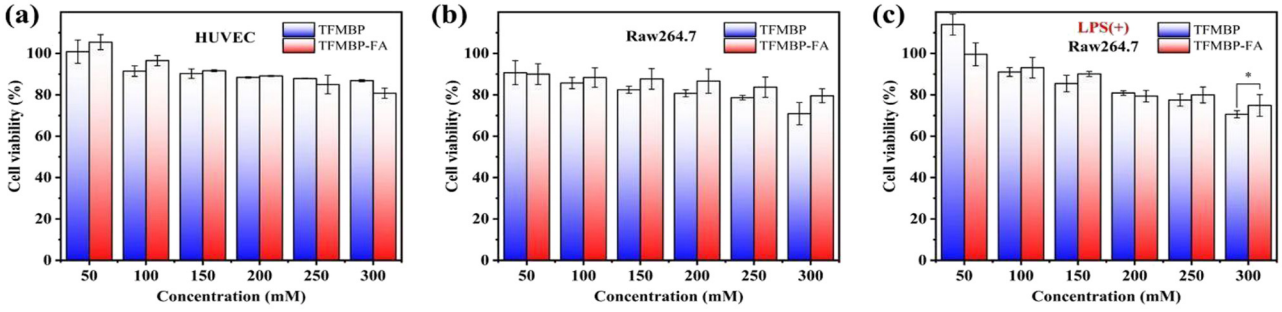

Figure 9: *In vitro*, cytotoxicity test of (a) HUVEC cells, (b) RAW 264.7 cells, and (c) activated RAW 264.7 cells in the presence of six different concentrations of TFMBP and TFMBP-FA.

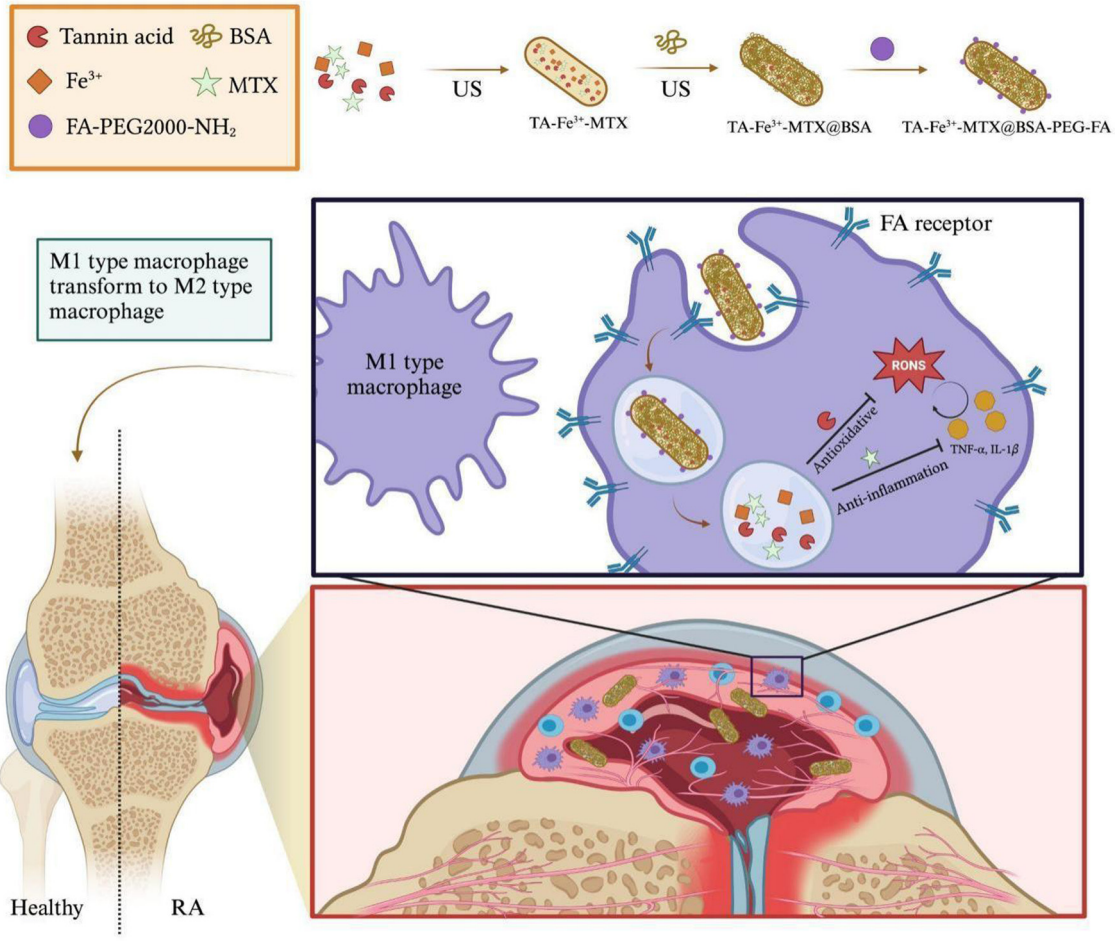

Figure 10: Schematic illustration of the synthesis of TFMBP and its application in RA therapy.

eliminate ROS was tested by a ROS detection kit (ROS Assay Kit), which uses the fluorescent probe DCFH-DA for ROS detection. DCFH-DA itself has no fluorescence and can freely pass through the cell membrane, and after entering the cell, it can be hydrolyzed by intracellular esterases to produce DCFH. However, DCFH cannot penetrate the cell membrane through DCFH, making it easy for probes to be loaded into cells. Reactive oxygen species in the cell can oxidize non-fluorescent DCF to form fluorescent DCF. The level of the fluorescence of DCF is directly related to the cell's ROS level [32].

RAW 264.7 cells were used and divided into six experimental groups. In the confocal images, LPS+, the activated macrophages, had significant bright and intense fluorescence (Figure 11a). LPS−, TFMBP-FA with activated macrophages, and TFMBP and TFMBP-FA with normal macrophages had barely visible fluorescence and low DCF density. TFMBP with activated macrophages had more visible fluorescence and low but relatively higher DCF density than LPS (Figure 11a). The significant high and low fluorescence intensities of LPS+TFMBP and LPS+TFMBP-FA were also displayed in Figure 11b. In LPS−, the subtle fluorescence intensity indicates the ROS originally contained in normal macrophages. In the inflammatory M1 macrophages, both TFMBP and TFMBP-FA had significant differences with LPS+, indicating the nanoparticles could eliminate ROS and turn M1 macrophage into M2 macrophage. The fluorescence intensity of LPS+TFMBP-FA was lower than LPS+TFMBP. Active targeting by folic acid increases the uptake of nanoparticles by the cells; increasing the uptake would eliminate more ROS. TFMBP could not eliminate the ROS in those cells that did not take in nanoparticles.

3.6 Anti-inflammation of TA-Fe^{3+}-MTX@BSA-PEG-FA

Inflammatory factors like cytokines deteriorate inflammation and symptoms of RA. The capability of TFMBP-FA to reduce the inflammatory factors was tested using a quantitative PCR (qPCR) and enzyme-linked immunosorbent

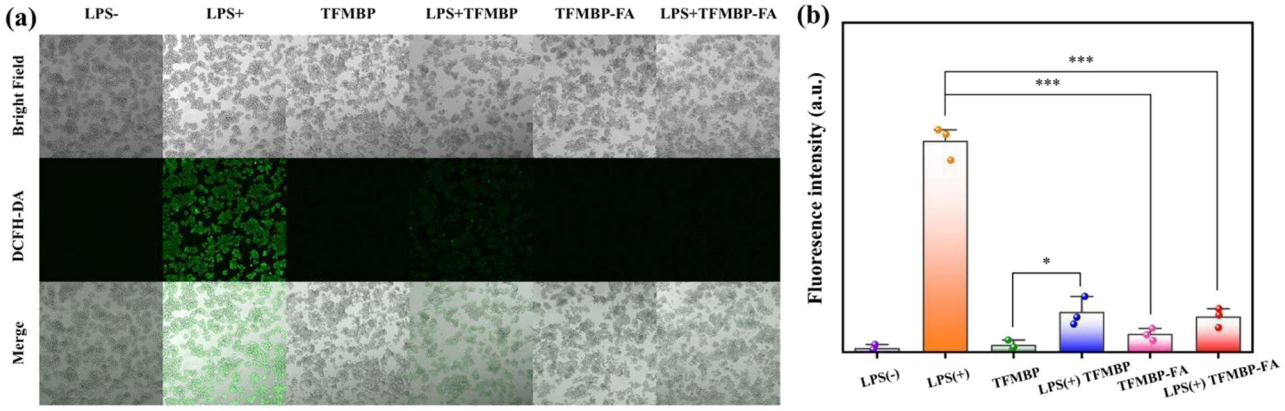

Figure 11: (a) Fluorescent confocal microscopy images of RAW 264.7 cells and activated RAW 264.7 cells with different treatments and then stained with ROS fluorescent probe DCFH-DA. (b) Quantified fluorescence intensity from flow cytometry. Statistics are reported as mean ± standard deviation (SD), $n = 3$. ***$p < 0.001$.

assay (ELISA) kit [33]. ELISA kit is used to detect the antibody of TNF-α and IL-1β in the cell solution. For accurate detection, measurement, and confirmation of anti-inflammatory effects, the IL-1 detection antibody is employed in inflammation scavenging research. It accurately measures IL-1β levels, enabling thorough examination and cross-sample comparison, and improves sensitivity and specificity with the slightest disturbance. RAW 264.7 cells were used for the experiment and separated into five experimental groups (LPS+, TFMBP, LPS+TFMBP, TFMBP-FA, and LPS+TFMBP-FA). The antibodies in the ELISA kit would bind to TNF-α and IL-1β, which would turn yellow after adding TMB ELISA substrate solution and H_2SO_4. The expression level of the antibody was indirectly related to the capability to eliminate inflammatory factors.

In the experiment of TNF-α, LPS+'s relative expression level of inflammatory factors reaches 90. LPS+TFMBP and LPS+TFMBP-FA reach the relative expression level of ~10. After using the nanoparticle, the expression level decreases nine times (Figure 12a). Similarly, in the IL-1β experiment, the relative expression level of LPS+ was around 90. In TFMBP with LPS, the relative expression level was about 15, 6 times lower than LPS+. The relative expression level of inflammatory factors was even lower in the LPS+TFMBP-FA group, which is around 5. LPS+ was 18 times larger than that (Figure 12b). After being treated with nanoparticles, the expression levels of the inflammatory factors decreased significantly. Lower levels of inflammatory factors would gradually reduce the vicious cycle of the RA microenvironment (Figure 2) [34]. The change in the expression level of inflammatory factors before (LPS+) and after (LPS+TFMBP-FA) the treatment of nanoparticles proved to have a therapeutic effect on RA. The data suggest that downregulated inflammatory cytokines indicate that TFMBP-FA nanoparticles have an inhibitory effect on inflammatory pathways and can alleviate inflammatory symptoms.

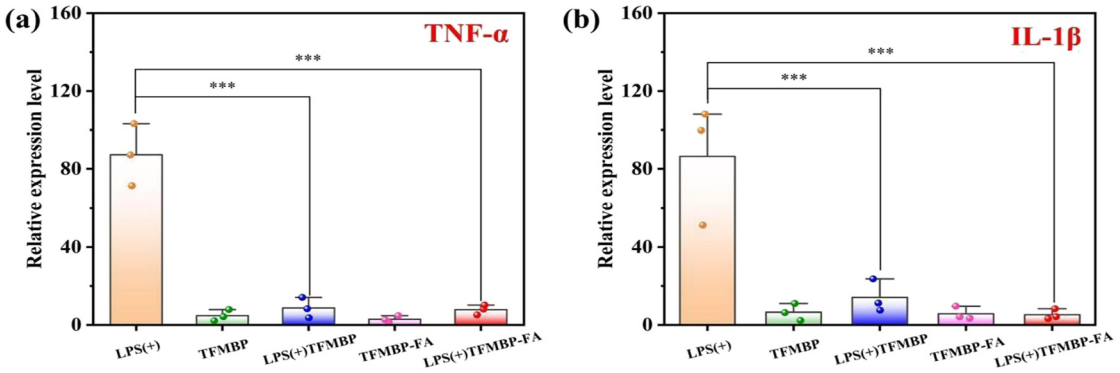

Figure 12: The mRNA levels of (a) TNF-α in activated RAW 264.7 cells treated with LPS+, TFMBP, LPS+TFMBP, TFMBP-FA, and LPS+TFMBP-FA, and (b) IL-1β in activated RAW 264.7 cells treated with LPS+, TFMBP, LPS+TFMBP, TFMBP-FA, and LPS+TFMBP-FA. Statistics are reported as mean ± standard deviation (SD), $n = 3$. ***$p < 0.001$.

4 Conclusions

In summary, TFMBP-FA was developed and expected to be an effective new drug in targeted RA therapy. TFMBP-FA can reduce inflammation by eliminating ROS and decreasing inflammatory factor levels. The statistical data showed that the tannin acid released by the nanoparticle plays a vital role in the treatment, which can remove ROS to relieve the three main pathological features. As an anti-inflammation medicine, MTX can be directly delivered to the inflamed joints to reduce the inflammatory factors, which is a critical step in alleviating inflammation. FA anchored around the surface enables nanoparticles to be actively targeted to M1-type macrophages in the inflamed joints. Active targeting enabled MTX to be directly sent to joint inflammation, reducing the interaction with other organs and diminishing the side effects. TFMBP-FA was developed to have surface stability and homogeneity, which enable biological application with high biosafety. The cytotoxicity was low at 50 mM with a cell viability rate of 99%, which proved the safety of TFMBP-FA. In future studies, animal experiments can be done on inflamed mice. The animal experiment evaluate the therapeutic efficiency and long-term toxicology of the nanoparticle. By continuing the exploration, this innovative treatment holds the potential to provide new hope in the battle against RA.

Acknowledgments: I would like to express my sincere appreciation to everyone who helped me, as their contributions and support have greatly enhanced the quality and rigor of this research. First and foremost, I am grateful to my primary advisor Dr. Xu for his unwavering guidance, insights, and constant encouragement throughout the research period. His expertise and wisdom were invaluable, always assisting me in overcoming obstacles during the most challenging phases of the project. Also, I would like to express my gratitude to my school advisor Mrs. Aidoo for all the support, instructions, and encouragement I received throughout this difficult project. I am grateful to the Suzhou Institute of Nano-Tech and Nano-Bionics and The Spence School for offering facilities and resources for this project. Their support facilitated the smooth execution of the research. I extend my appreciation to my friends, who have been supportive throughout and provided a stimulating academic environment. Their encouragement was immensely motivating during my challenging research journey. Lastly, I am thankful to my family for their understanding, encouragement, and support.

Funding information: The author states no funding involved.

Author contributions: Xinran Ma designed the framework, analyzed the performance, validated the results, and wrote the article. The author has accepted responsibility for the entire content of this manuscript and approved its submission.

Conflict of interest: The author states no conflict of interest.

References

[1] Xu Y, Wu Q. Prevalence trend and disparities in rheumatoid arthritis among US adults, 2005–2018. J Clin Med. 2021;10(15):3289.
[2] Smolen JS, Aletaha D. Challenges of predicting treatment response in patients with rheumatoid arthritis. Nat Clin Pract Rheumatol. 2005;1(2):62–3.
[3] Cush JJ. Rheumatoid arthritis: Early diagnosis and treatment. Rheum Dis Clin North Am. 2022;48(2):537–47.
[4] Burmester GR, Pope JE. Novel treatment strategies in rheumatoid arthritis. Lancet. 2017;389(10086):2338–48.
[5] Abbasi M, Mousavi MJ, Jamalzehi S, Alimohammadi R, Bezvan MH, Mohammadi H, et al. Strategies toward rheumatoid arthritis therapy: The old and the new. J Cell Physiol. 2019;234(7):10018–31.
[6] England BR, Thiele GM, Anderson DR, Mikuls TR. Increased cardiovascular risk in rheumatoid arthritis: mechanisms and implications. Bmj. 2018;361:k1036.
[7] Zhu Y, Zhao T, Liu M, Wang S, Liu S, Yang Y, et al. Rheumatoid arthritis microenvironment insights into treatment effect of nanomaterials. Nano Today. 2022;42:101358.
[8] Yang Y, Guo L, Wang Z, Liu P, Liu X, Ding J, et al. Targeted silver nanoparticles for rheumatoid arthritis therapy via macrophage apoptosis and Re-polarization. Biomaterials. 2021;264:120390.
[9] Zhao J, Jiang P, Guo S, Schrodi SJ, He D. Apoptosis, autophagy, NETosis, necroptosis, and pyroptosis mediated programmed cell death as targets for innovative therapy in rheumatoid arthritis. Front Immunol. 2021;12:809806.
[10] Pucci C, Martinelli C, De Pasquale D, Battaglini M, di Leo N, Degl'Innocenti A, et al. Tannic acid–iron complex-based nanoparticles as a novel tool against oxidative stress. ACS Appl Mater Interfaces. 2022;14(14):15927–41.
[11] Yu M, Sun X, Dai X, Gu C, Gu M, Wang A, et al. Effects of tannic acid on antioxidant activity and ovarian development in adolescent and adult female Brandt's voles. Reprod Sci. 2021;28:2839–46.
[12] Li M, Liu P, Xue Y, Liang Y, Shi J, Han X, et al. Tannic acid attenuates hepatic oxidative stress, apoptosis and inflammation by activating the Keap1-Nrf2/ARE signaling pathway in arsenic trioxide-toxicated rats. Oncol Rep. 2020;44(5):2306–16.
[13] Guo L, Zhong S, Liu P, Guo M, Ding J, Zhou W. Radicals scavenging MOFs enabling targeting delivery of siRNA for rheumatoid arthritis therapy. Small. 2022;18(27):2202604.
[14] Brzezicka KA, Arlian BM, Wang S, Olmer M, Lotz M, Paulson JC. Suppression of autoimmune rheumatoid arthritis with hybrid nanoparticles that induce B and T cell tolerance to self-antigen. ACS Nano. 2022;16(12):20206–21.
[15] Xie L, Zhang N, Zhang Q, Li C, Sandhu AF, Williams G, III, et al. Inflammatory factors and amyloid β-induced microglial

polarization promote inflammatory crosstalk with astrocytes. Aging (Albany NY). 2020;12(22):22538.
[16] Yan F, Zhong Z, Wang Y, Feng Y, Mei Z, Li H, et al. Exosome-based biomimetic nanoparticles targeted to inflamed joints for enhanced treatment of rheumatoid arthritis. J Nanobiotechnol. 2020;18:1–5.
[17] Li H, Feng Y, Zheng X, Jia M, Mei Z, Wang Y, et al. M2-type exosomes nanoparticles for rheumatoid arthritis therapy via macrophage re-polarization. J Controll Release. 2022;341:16–30.
[18] Lv R, Bao Q, Li Y. Regulation of M1-type and M2-type macrophage polarization in RAW264. 7 cells by Galectin-9. Mol Med Rep. 2017;16(6):9111–9.
[19] Solomon DH, Giles JT, Liao KP, Ridker PM, Rist PM, Glynn RJ, et al. Reducing cardiovascular risk with immunomodulators: A randomised active comparator trial among patients with rheumatoid arthritis. Ann Rheum Dis. 2023;82(3):324–30.
[20] Wang Q, Qin X, Fang J, Sun X. Nanomedicines for the treatment of rheumatoid arthritis: State of art and potential therapeutic strategies. Acta Pharm Sin B. 2021;11(5):1158–74.
[21] Wen J, Li H, Dai H, Hua S, Long X, Li H, et al. Intra-articular nanoparticles based therapies for osteoarthritis and rheumatoid arthritis management. Mater Today Bio. 2023;19:100597.
[22] Veerappermal Devarajan M. Assessing long-term serum sample viability for cardiovascular risk prediction in rheumatoid arthritis. Int J Inf Technol Comput Eng. 2020;8(2):2347–57.
[23] Zinke M, Lejeune M, Mechaly A, Bardiaux B, Boneca IG, Delepelaire P, et al. Ton motor conformational switch and peptidoglycan role in bacterial nutrient uptake. Nat Commun. 2024;15(1):331.
[24] Clogston JD, Patri AK. Zeta potential measurement. Characterization of nanoparticles intended for drug delivery. Methods in Molecular Biology. Humana Press; 2011. p. 63–70.
[25] Clayton KN, Salameh JW, Wereley ST, Kinzer-Ursem TL. Physical characterization of nanoparticle size and surface modification using particle scattering diffusometry. Biomicrofluidics. 2016;10:054107.
[26] Kiefer J, Grabow J, Kurland HD, Müller FA. Characterization of nanoparticles by solvent infrared spectroscopy. Anal Chem. 2015;87(24):12313–7.
[27] Ramachandran VS, Beaudoin JJ. Handbook of analytical techniques in concrete science and technology: principles, techniques and applications. Norwich, New York, USA: Elsevier; 2000.
[28] Shah VP, Miron DS, Rădulescu FȘ, Cardot JM, Maibach HI. In vitro release test (IVRT): Principles and applications. Int J Pharm. 2022;626:122159.
[29] Barbillon G. Plasmonics and its applications. Materials. 2019;12(9):1502.
[30] Yang X, Zhong Y, Wang D, Lu Z. A simple colorimetric method for viable bacteria detection based on cell counting Kit-8. Anal Methods. 2021;13(43):5211–5.
[31] Fedr R, Kahounová Z, Remšík J, Reiterová M, Kalina T, Souček K. Variability of fluorescence intensity distribution measured by flow cytometry is influenced by cell size and cell cycle progression. Sci Rep. 2023;13(1):4889.
[32] Gao C, Wang Q, Ding Y, Kwong CH, Liu J, Xie B, et al. Targeted therapies of inflammatory diseases with intracellularly gelated macrophages in mice and rats. Nat Commun. 2024;15(1):328.
[33] Mousa ZS, Abdulamir AS. Application and validation of SARS-CoV-2 RBD neutralizing ELISA assay. Arch Razi Inst. 2022;77(1):391–402.
[34] Choy EH, Kavanaugh AF, Jones SA. The problem of choice: Current biologic agents and future prospects in RA. Nat Rev Rheumatol. 2013;9(3):154–63.